Volume 6 | Number 6 | 21 March 2022

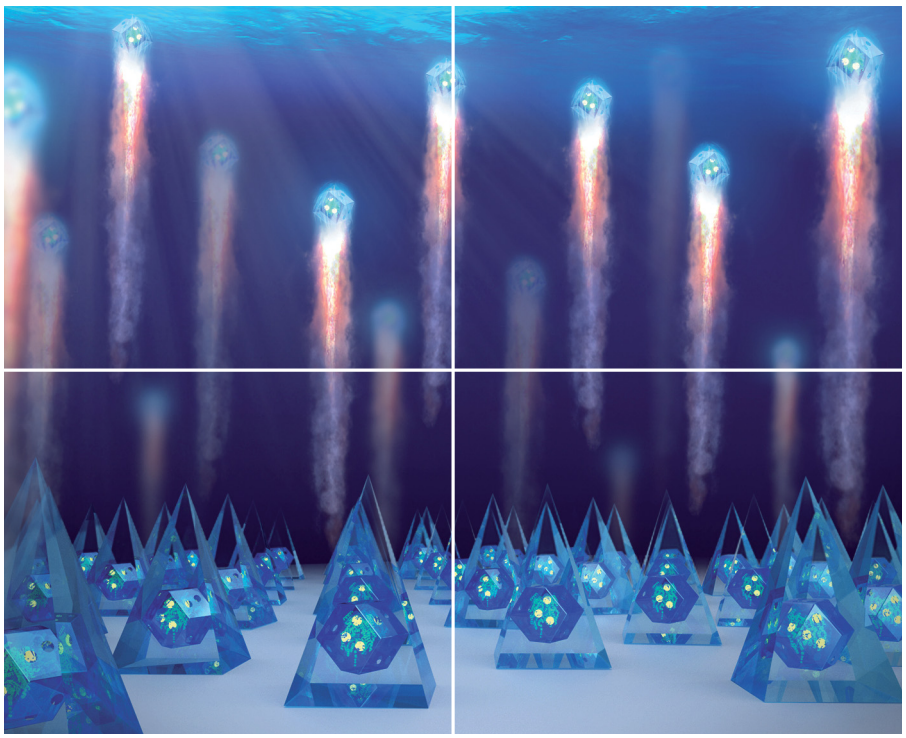

MATERIALS CHEMISTRY

FRONTIERS

CCS 中国化学会 CHINESE CHEMICAL SOCIETY

ICCAS 1956

ROYAL SOCIETY OF CHEMISTRY

rsc.li/frontiers-materials

MATERIALS CHEMISTRY FRONTIERS

CCS 中国化学会 CHINESE CHEMICAL SOCIETY

ICCAS

ROYAL SOCIETY OF CHEMISTRY

RESEARCH ARTICLE

View Article Online
View Journal | View Issue

Cite this: *Mater. Chem. Front.*, 2022, **6**, 680

Hierarchically porous MOF-based microneedles for glucose-responsive infected diabetic wound treatment†

Xiao-Xi Yang,[a] Yan-Li Chen,[b] Peng-Fei Feng,[a] Cong-Cong Wang,[a] Xiang-Kai Li,[b] Liang-Liang Liu*[a] and Yu Tang *[a]

Received 12th November 2021,
Accepted 5th January 2022

DOI: 10.1039/d1qm01512e

rsc.li/frontiers-materials

Elaborately designed stimuli-responsive antibacterial systems are highly desirable for infected diabetic wound treatment. Herein, hierarchically porous metal–organic framework (MOF)-based glucose-responsive microneedles (MNs) were designed for painless transdermal wound treatment. For the first time, a hierarchically porous MOF was applied for consuming the surplus glucose to protect infected diabetic wounds from bacterial infection. Through one-pot synthesis, glucose oxidase (GOx) was firstly encapsulated into a Fe-doped zeolitic imidazolate framework (ZIF), and based on a properly controlled tannic acid (TA) etching process, the hierarchically porous MOF (GOx@Fe-ZIF-TA) was constructed afterwards. GOx encapsulated in GOx@Fe-ZIF-TA could consume surplus glucose in infected diabetic wounds to yield gluconic acid and H_2O_2. The latter could be catalyzed by Fe(II) to generate antibacterial •OH, which would not result in antimicrobial resistance. The as-obtained hierarchically porous MOF revealed satisfactory glucose-responsive antibacterial activity, and the hierarchically porous MOF-based MNs showed enough stiffness for penetration. This study offers a new strategy, using hierarchically porous enzyme-loaded MOFs as depots to integrate with MNs, for designing stimuli-responsive transdermal systems for the treatment of infected diabetic wounds and other diseases.

Introduction

Metal–organic frameworks (MOFs) have shown great potential in many fields like catalysis, sensing, gas separation and biomedical research.[1–5] In biomedical research, various biomolecules such as enzymes and vaccines have been embedded in MOF matrices to enhance their stability or activity.[6–14] Additional studies focused on using ZIF-8, a nontoxic and biocompatible zeolitic imidazolate framework (ZIF), as the MOF matrix to encapsulate enzymes through one-pot synthesis to construct stimuli-responsive systems.[15–17] However, the enzyme activity may be disturbed by this coprecipitation or biomineralization strategy. On the one hand, the steric trapping may result in the change of the enzyme conformation.[9,18,19] On the other hand, the interaction between MOFs and enzymes may alter the native state of enzymes.[20,21] Recent research studies have shown that hierarchically porous MOFs could improve substrate diffusion and enable the encapsulation of guest bio-macromolecules in their relatively free state at the same time.[22,23]

Etching is a promising method for the fabrication of hierarchically porous MOFs.[24] Tannic acid (TA), as an etching agent, could be used to facilely generate voids within ZIF matrices to construct hierarchically porous structures.[25–27] Meanwhile, TA could be coated on the MOF surface during the etching process, which could play an important role in antibacterial or anticancer treatment.[28] For example, by combining with glucose oxidase (GOx, a common enzyme which could consume glucose and O_2 to yield gluconic acid and H_2O_2) embedded in ZIFs, TA could convert Fe(III) in the particles to Fe(II) which would decompose H_2O_2 to generate ROS based on the Fe-mediated Fenton reaction for biomedical treatment.[16] The other cases also proved that TA could convert Fe(III) to Fe(II) and could be applied for the generation of ROS based on a Fenton-like reaction.[29,30] For wound infection treatment, unlike antibiotics or other antibacterial molecules, ROS would not result in antimicrobial resistance and have been widely researched.[31,32] Nonetheless, previous reports usually needed external H_2O_2 for the ROS generation. Diabetic wounds, usually resulting from uncontrolled blood glucose levels, are also susceptible to bacterial infection.[33] For such wounds, the

[a] *Key Laboratory of Nonferrous Metal Chemistry and Resources Utilization of Gansu Province, College of Chemistry and Chemical Engineering, Lanzhou University, Lanzhou 730000, P. R. China. E-mail: tangyu@lzu.edu.cn, liull@lzu.edu.cn*

[b] *Ministry of Education Key Laboratory of Cell Activities and Stress Adaptations, School of Life Sciences, Lanzhou University, Lanzhou 730000, P. R. China*

† Electronic supplementary information (ESI) available: Supporting tables and figures. See DOI: 10.1039/d1qm01512e

wound healing process could be accelerated by simultaneously decreasing the glucose levels and protecting the wounds from bacterial infection,[34] which makes GOx-involved systems promising candidates for infected diabetic wound treatment.

The use of MNs has been proved to be a promising medical technique for the treatment of many diseases including skin infection, cancer, diabetes, and so on.[35,36] With needles usually less than 1 mm, MNs can penetrate through the epidermis painlessly. Thus, different kinds of drugs or vehicles could be delivered into specific sites. For skin infection treatment, methods in the form of gels, creams, and ointments containing antimicrobial agents are most widely preferred.[37] However, these methods are usually limited by the inefficient penetration of antibacterial agents through the extracellular polymeric substances into the biofilm, and thus have low effectiveness to reach bacteria in the deep sites.[38] MNs could effectively penetrate into the biofilm and release antibacterial agents deep inside the biofilm. This advantage makes the use of MNs an ideal technique for infected wound treatment. Furthermore, various kinds of molecules or particles have been combined with MNs for stimuli-responsive antibacterial treatment, including localized pH change or heat *via* infrared radiation.[39] Yet, the combination of MOFs and MNs for the glucose-responsive treatment of infected diabetic wounds has never been reported.

Herein, a hierarchically porous MOF (GOx@Fe-ZIF-TA) was constructed and encapsulated into dissolvable polyvinyl pyrrolidone (PVP) to fabricate stimuli-responsive microneedles for infected diabetic wound treatment. For the first time, a hierarchically porous MOF was applied for consuming the surplus glucose to protect infected diabetic wounds from bacterial infection. As illustrated in Scheme 1, GOx was firstly encapsulated into a Fe-doped ZIF through one-pot synthesis, and the hierarchically porous MOF was constructed afterwards based on a properly controlled TA etching process. TA was used to etch the MOF to construct hierarchically pores and offer Fe(II)/Fe(III) redox conversion. When MNs were applied on the wound site, the GOx@Fe-ZIF-TA particles would be released from PVP, and sequentially GOx would consume glucose to yield H_2O_2 and gluconic acid. Under the local acidic environment produced by gluconic acid, Fe(III) would be reduced to Fe(II) by TA and further catalyze the degradation of H_2O_2 to produce antibacterial $^{\bullet}OH$. The as-obtained hierarchically porous MOF revealed satisfactory glucose-responsive antibacterial activity, and the hierarchically porous MOF-based MNs showed enough stiffness for penetration.

Experimental section

Materials and chemicals

Zinc nitrate, ferrous chloride, 2-methylimidazole and porcine skin were purchased from Lanzhou Aihua Co., Ltd. Glucose, glucose oxidase, fluorescein isothiocyanate (FITC), and

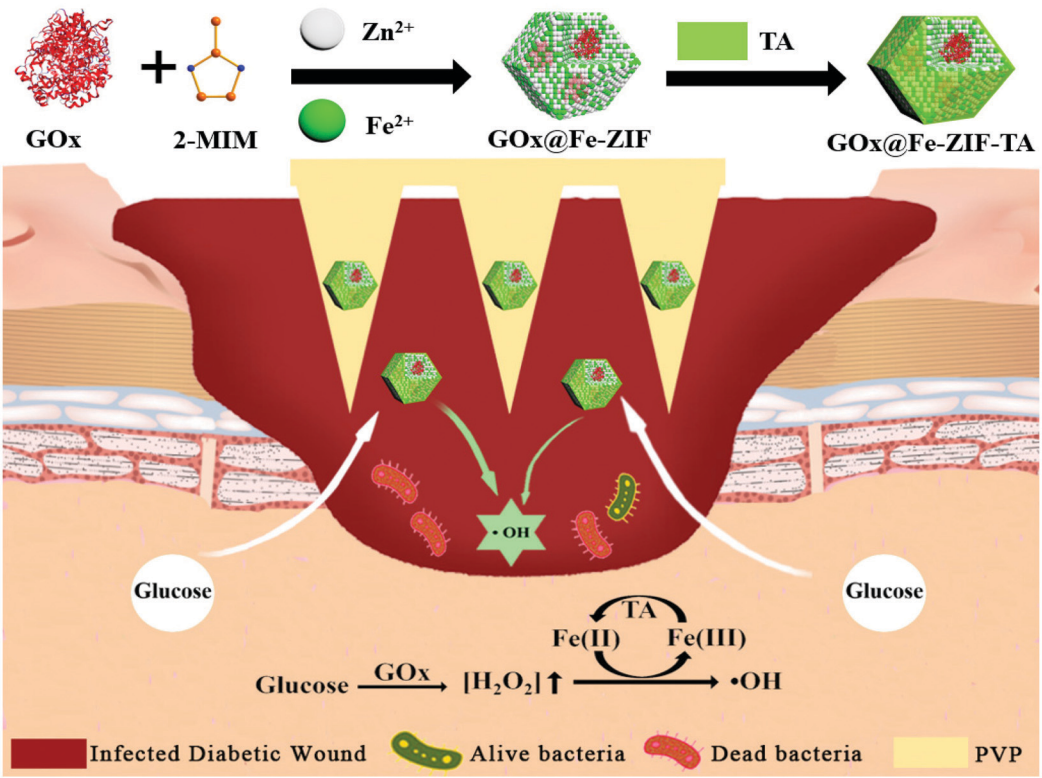

Scheme 1 Schematic illustration of preparation of hierarchically porous glucose-responsive antibacterial GOx@Fe-ZIF-TA and penetration of MOF-based MNs into infected diabetic wounds to release antibacterial particles for infected diabetic wound treatment.

poly-vinylpyrrolidone PVP (M_w: 10 kDa) were purchased from Heowns (Tianjin, China). The PDMS mold was purchased from Taizhou Microchip Pharmaceutical Technology Co., Ltd.

Synthesis and characterization of a hierarchically porous MOF

GOx@Fe-ZIF-TA was synthesized through a modified two step reaction.[15,23,40] Firstly, GOx@Fe-ZIF was synthesized by mixing GOx (200 μg), 2-methylimidazole (1 mL, 1.4 M), zinc nitrate (0.97 mL, 20 mM) and ferrous chloride (0.3 mL, 20 mM). After overnight reaction, GOx@Fe-ZIF was obtained by centrifugation and washing with water. Secondly, GOx@Fe-ZIF-TA was obtained through a modified etching process by mixing TA with the suspension solution of GOx@Fe-ZIF for 2 min, followed by centrifugation and washing with water. The encapsulation efficiency of GOx in GOx@Fe-ZIF and GOx@Fe-ZIF-TA was determined by fluorescence spectrophotometry (RF5301-PC, Shimadzu) using a calibration curve of FITC-modified GOx. The morphology of GOx@Fe-ZIF and GOx@Fe-ZIF-TA was visualized *via* scanning electron microscopy (SEM, S-4800, Hitachi) and transmission electron microscopy (TEM, Talos F200s; FEI Company). A laser scanning confocal microscope (A1R MP, Nikon) was used to confirm the encapsulation of FITC-modified GOx. XRD patterns were achieved on a Rigaku D/Max-2400. Fourier transform infrared (FT-IR) spectra were recorded on a Nicolet 360 FTIR spectrometer using the KBr pellet method. BET tests were carried on a Micromeritics ASAP2460.

Glucose-responsive catalytic activity assay

The catalytic activity was probed by monitoring the degradation of methylene blue (MB) in glucose solution. Briefly, certain amounts of GOx@ZIF-TA, GOx@ZIF@Fe-TA and GOx@Fe-ZIF-TA were dispersed into the solution containing the same concentration of MB and glucose (15 mM, corresponding to the blood glucose concentration in diabetic patients). To investigate the glucose-responsive behavior, GOx@Fe-ZIF-TA was dispersed into the solution containing the same concentration of MB and different concentrations of glucose (0 mM, 5 mM (normal blood glucose concentration), and 15 mM). UV-vis absorption of MB was acquired on a Cary 5000 (Cary-5000, Agilent technologies). The glucose-responsive ROS generation of GOx@Fe-ZIF-TA was probed *via* the EPR signal of DMPO–OH (ER200DSRC10/12, Bruker).

In vitro glucose-responsive antibacterial tests

Briefly, *Escherichia coli* (ATCC 8739) was divided into four groups: bacteria + low concentration glucose (5 mM), bacteria + high concentration glucose (15 mM), bacteria + low concentration glucose (5 mM) + GOx@Fe-ZIF-TA (50 μg mL^{-1}), and bacteria + high concentration glucose (15 mM) + GOx@Fe-ZIF-TA (50 μg mL^{-1}). After incubation, the antibacterial activity was evaluated by the number of colonies left on the Petri dish.

MNs fabrication

MNs were fabricated using the micromolding technology. Briefly, 1.5 mg of GOx@Fe-ZIF-TA was added to 1 mL mixed solution of PVP and PVA (PVP : PVA = 3 : 1). After being stirred, the final solution was poured onto the PDMS template. Then the template was placed in a vacuum for 30 min. After drying, the MNs were carefully peeled off. A fluorescence microscope (Ts2-FL, Nikon) was used to characterize the distribution of GOx@Fe-ZIF-TA by probing FITC-modified GOx loaded inside the particle.

Mechanical strength study

An automatic load tester was used to test the mechanical strength of MNs (Hssdtest, UTM4104, China). The movement speed of the plate to MNs was set to be 0.5 mm s^{-1}. Porcine skin was also used to investigate the mechanical strength of MNs. Briefly, with a pressure of 5.0 N, MNs were applied onto the porcine skin. Then the MNs were peeled off and then put into the glutaraldehyde solution. After that, the porcine skin was dried and coated with gold for SEM tests.

Results and discussion

Characterization of a hierarchically porous MOF

GOx@Fe-ZIF-TA was synthesized through a modified two step reaction (Scheme 1). The GOx@Fe-ZIF precursor was synthesized by mixing GOx, 2-methylimidazole, zinc nitrate and ferrous chloride, and then TA was used to etch GOx@Fe-ZIF to construct hierarchically porous GOx@Fe-ZIF-TA. Through a one-pot reaction, various metal ions have been introduced into the system to partially replace Zn(II) during the growth of ZIF particles.[17,40] TEM and SEM images showed that the resulting GOx-loaded Fe-doped particles (GOx@Fe-ZIF) before TA treatment revealed a dodecahedral structure, along with a grain size of 200–800 nm (Fig. 1a). The elemental mapping images of GOx@Fe-ZIF clearly exhibited the distribution of Zn, Fe, and N, which not only confirmed the successful loading of GOx into the MOF but also indicated the uniform distribution of Fe before TA etching (Fig. S1, ESI†). After the TA etching process, GOx@Fe-ZIF-TA revealed a similar dodecahedral structure and particle size to GOx@Fe-ZIF, and obvious voids could be observed, which is in agreement with previous reports (Fig. 1b).[23,25] The elemental mapping images of GOx@Fe-ZIF-TA revealed the distribution of Zn, Fe, and N elements in the unapparent outer shell (Fig. 1c). It should be noted that the shell can become more obvious with the increase of etching time (Fig. S2, ESI†). However, for complete etching with a longer TA etching time, excessive TA would coat the MOF surface and it would also result in enzyme aggregation because of the overly expanded space as demonstrated previously, which would reduce the catalytic efficiency.[25,27,41] Meanwhile, insufficient etching in our case would not provide overly expanded space for enzyme-catalyzed reactions.[23] The loadings of GOx in GOx@Fe-ZIF and GOx@Fe-ZIF-TA were measured to be 11.0 μg mg^{-1} and 10.5 μg mg^{-1}, respectively. This indicated the negligible GOx leaching during the TA etching process. CLSM images (Fig. 1d) also confirmed that GOx was successfully retained in the GOx@Fe-ZIF-TA.

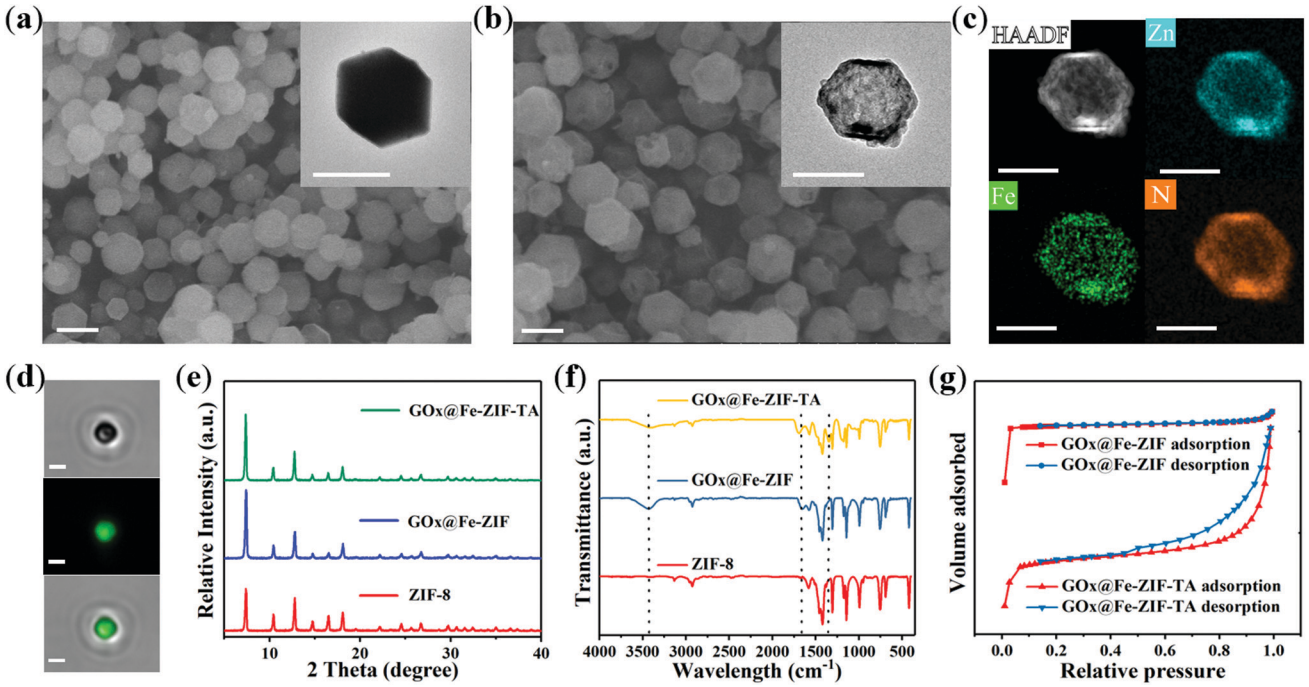

Fig. 1 (a) SEM and TEM (inserted at the corner) images of GOx@Fe-ZIF. (b) SEM and TEM (inserted at the corner) images of GOx@Fe-ZIF-TA. (c) Elemental mapping images of GOx@Fe-ZIF-TA. (d) Confocal microscopy images of GOx@Fe-ZIF-TA (probing the green fluorescence of FITC-modified GOx). (e) XRD patterns of samples. (f) FT-IR spectra of samples. (g) N_2 adsorption–desorption isotherms of GOx@Fe-ZIF and GOx@Fe-ZIF-TA (all scale bars: 500 nm).

Before TA etching, Fe(II) partially replaces Zn(II) and chemically bonds with imidazolate within the ZIF, which is in good agreement with the powder X-ray diffraction (PXRD) pattern (Fig. 1e), and after the TA etching process, the ZIF crystal structure could still be well preserved. Fourier-transform infrared spectroscopy (FT-IR) spectra (Fig. 1f) revealed that after TA etching treatment, compared to GOx@Fe-ZIF, two extra adsorption bands emerge at $\sim$1340 cm^{-1} and 1700 cm^{-1} for GOx@Fe-ZIF-TA, corresponding to the C–O vibrations and C═O stretching of TA, indicating the successful coating of TA on GOx@Fe-ZIF, which is in good agreement with the previous report.[23] Also, the broad adsorption band at 3400 cm^{-1} indicated the existence of O–H, revealing the successful encapsulation of GOx in the MOF and good preservation after the etching process. BET tests were applied to investigate the formation of a hierarchically porous structure of GOx@Fe-ZIF-TA. As can be seen in Fig. 1g, after the TA etching process, the N_2 adsorption of GOx@Fe-ZIF-TA was steady at low relative pressure, which indicated that the main microporosity of the ZIF was not destroyed in the etching process. However, compared with GOx@Fe-ZIF, a distinct hysteresis loop of GOx@Fe-ZIF-TA emerged at high relative pressure, which confirmed the generation of mesopores in GOx@Fe-ZIF-TA by etching and the successful preparation of hierarchically porous MOF.[23] Also, compared with GOx@Fe-ZIF, GOx@Fe-ZIF-TA showed a decreased microporous volume to total pore volume ratio (Table S1, ESI†), further confirming the successful etching of TA. In Fe-mediated Fenton reaction systems, Fe(II) exhibits higher catalytic performance than Fe(III) for catalyzing H_2O_2 to produce ROS.[42] It has to be noted that Fe(II) doped in GOx@Fe-ZIF can be easily converted to Fe(III) by the O_2 in the air before the etching process. XPS patterns (Fig. S3, ESI†) showed that after the overnight reaction, most of the Fe(II) doped in the ZIF has been oxidized into Fe(III).[30] However, in our system, GOx would consume glucose to yield H_2O_2 and gluconic acid, and in the local acidic environment produced by gluconic acid, and TA could accelerate the conversion from Fe(III) (low catalytic efficiency) to Fe(II) (high catalytic efficiency) for the Fenton reaction like previous reports.[16,29]

To achieve the optimal molar ratio of Fe : Zn, various amounts of Fe were introduced into the system to achieve GOx@Fe-ZIF precursors. The SEM images showed that the amount of Fe had a significant influence on the morphology of GOx@Fe-ZIF (Fig. S4, ESI†). When the molar ratio of Fe : Zn was lower than 4 : 96, the resulting MOF still revealed a rhombic dodecahedral structure. Once the molar ratio of Fe : Zn increased from 6 : 94 to 10 : 90, more and more impurities emerged and the dodecahedral structure of the MOF became less and less obvious. This indicated that the excess Fe would have a bad influence on the growth of ZIF-crystals. BET tests were further carried out to investigate the influence of Fe on the MOF structure. As displayed in Table S2 (ESI†), when the Fe content was lower than 3%, the micropore content did not show significant change with the increase of the Fe amount. However, when Fe content was higher than 4%, the micropore content would decrease significantly with the increase of the Fe amount. The decrease of micropores in GOx@Fe-ZIF could be attributed to the excess Fe having a bad influence on the growth

of ZIF-crystals, and such unexpected mesopores might provide the overly expanded space for enzyme aggregation, which would reduce the efficiency of enzyme-catalytic reaction. In our system, the total catalytic efficiency was determined by two catalytic reactions, which are the catalytic reaction of glucose oxidase and the Fenton reaction of Fe. The catalytic efficiency of the Fenton reaction was affected by the amount of Fe, and it would increase with the increase of Fe content. To precisely control the etching process for hierarchically porous structure and maintain the highest catalytic efficiency, the molar ratio of Fe : Zn was chosen to be 3 : 97.

Glucose-responsive catalytic activity assay

In our system, GOx in the hierarchically porous MOF could convert glucose and O_2 to gluconic acid and H_2O_2. The gluconic acid could produce an acidic environment for the conversion of Fe(III) to Fe(II), and sequentially the H_2O_2 would be catalyzed to produce ROS by Fe(II).[16] To investigate the influence of hierarchically pores on the catalytic efficiency of this glucose-responsive Fenton reaction, GOx@ZIF@Fe-TA with the same content of Fe was synthesized through a reported strategy for comparison (Fig. S5, ESI†).[16] Fig. 2a–c show the MB degradation spectra of GOx@ZIF-TA, GOx@ZIF@Fe-TA and GOx@Fe-ZIF-TA in 15 mM glucose solution, respectively. The time-dependent absorbances of MB at 664 nm are displayed in Fig. 2d for comparison. When Fe was not doped into the MOF matrix, GOx@ZIF-TA showed a limited ability to decompose MB because the yielded H_2O_2 could not be converted into highly oxidative ROS. However, the absorbance of MB decreased sharply when Fe was introduced into the system, which indicated the essential role of Fe in the catalytic reaction. The results also showed that GOx@Fe-ZIF-TA had a higher catalytic efficiency than GOx@ZIF@Fe-TA, which could be attributed to the appearance of hierarchical pores within the MOF matrix and sequentially improving the catalytic efficiency.[23] The etching time for GOx@ZIF@Fe-TA was controlled to be 10 min as reported, which is far more than the reaction time for GOx@Fe-ZIF-TA (2 min in our case). As shown in Fig. S5 (ESI†), such a complete etching process with long etching time would result in the hollow structure of the MOF and further cause enzyme aggregation in the overly expanded space, which would limit the enzyme activity.[25,27] However, in our research, the reaction time of TA treatment for GOx@Fe-ZIF-TA was controlled to be 2 min, and such an incomplete etching process with short etching time would not provide an overly expanded space for enzyme aggregation.[23] Noteworthily,

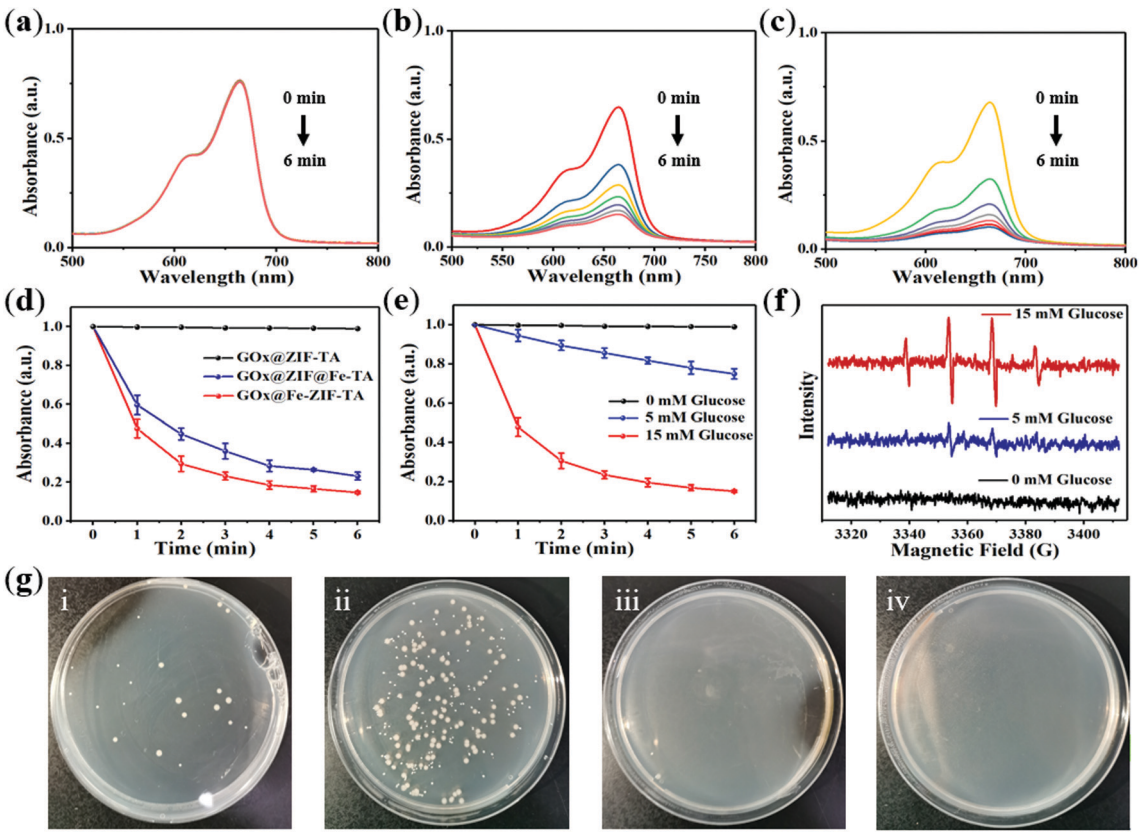

Fig. 2 MB degradation spectra of (a) GOx@ZIF-TA, (b) GOx@ZIF@Fe-TA and (c) GOx@Fe-ZIF-TA in glucose solution. (d) Time-dependent absorbance of MB at 664 nm of corresponding samples in glucose solution. (e) Time-dependent absorbance of MB at 664 nm of GOx@Fe-ZIF-TA in glucose solution with different concentrations. (f) EPR signals of corresponding samples in glucose solution (probing the signal of DMPO–OH). (g) *E. coli* incubated in (i) low concentration glucose, (ii) high concentration glucose, (iii) low concentration glucose + GOx@Fe-ZIF-TA and (iv) high concentration glucose + GOx@Fe-ZIF-TA.

the previously doped Fe could be beneficial to the etching process. This assumption was confirmed by TEM images of GOx@ZIF@Fe-TA and GOx@Fe-ZIF-TA at different time intervals during the etching process at the same concentration of TA. As shown in Fig. S6 (ESI†), without previously doped Fe, TA would slowly etch the GOx@ZIF uniformly from outside to inside. However, in our system with previously doped Fe, the TA etching process could be more efficient for the inner part of the MOF matrix. This could be because TA would preferentially react with Fe(III) instead of Zn(II) due to the stronger interaction between TA and Fe(III) compared with the interaction between TA and Zn(II) during the etching process.[43,44] Since Fe was uniformly distributed in GOx@Fe-ZIF, the etching reaction would take place more deeply compared to the one without the previous Fe-doping process within the same reaction time. Also, as shown in Table S1 (ESI†), GOx@Fe-ZIF-TA had a lower micropore volume to total pore volume ratio than GOx@ZIF@Fe-TA, which further confirmed that the previously doped Fe could enhance the etching effect.

Since the amount of H_2O_2 yielded is affected by the amount of glucose in the GOx-involved catalytic reaction, GOx@Fe-ZIF-TA was dispersed in various concentrations of glucose solutions to further investigate the glucose-responsive catalytic activity. MB degradation tests were also applied to reveal the catalytic activity of our system. As shown in Fig. 2e, when no glucose was added into the MB solution, GOx@Fe-ZIF-TA could not decompose MB without the existence of glucose in MB solution. With the increase of glucose concentration, MB could be decomposed more and more effectively, which well indicated the glucose-responsive catalytic efficiency of GOx@Fe-ZIF-TA. Also, the EPR tests were applied to reveal the glucose-responsive generation of •OH radicals. The results showed that GOx@Fe-ZIF-TA could generate ROS in a glucose-responsive manner. As can be seen from Fig. 2f, no ROS signal could be detected when GOx@Fe-ZIF-TA was dispersed into a solution without glucose. When a low concentration of glucose solution was applied, a relatively low •OH signal could be observed, and a stronger •OH signal could be detected when GOx@Fe-ZIF-TA was immersed in glucose solution at a high concentration. On the basis of the above results, our system could be applied for glucose-mediated antibacterial treatment.

In vitro glucose-responsive antibacterial tests

Escherichia coli (*E. coli*), as a common wound pathogen, was selected to investigate the glucose-responsive antibacterial activity of GOx@Fe-ZIF-TA. As shown in Fig. 2g(i) and (ii), when antibacterial GOx@Fe-ZIF-TA was not applied, a high concentration of glucose would result in the dramatic increase of the number of colonies as *E. coli* could consume glucose as the carbon source. When GOx@Fe-ZIF-TA was applied, for a low concentration of glucose (Fig. 2g(iii)), the number of colonies decreased but some colonies could still be observed, which indicated the limited antibacterial activity of GOx@Fe-ZIF-TA at a low concentration of glucose. This could be because a low amount of •OH was generated and TA itself has antibacterial activity.[28] However, when GOx@Fe-ZIF-TA was applied together with a high concentration of glucose (Fig. 2g(iv)), colonies could be no more observed, which indicated the excellent antibacterial activity of GOx@Fe-ZIF-TA at high concentration of glucose. These results confirmed that hierarchically porous GOx@Fe-ZIF-TA could kill pathogens in a glucose-responsive manner, which could be applied in infected diabetic wounds.

Characterization of hierarchically porous MOF-based MNs

MNs have shown great potential in infected wound treatment. By effectively penetrating into the biofilm at the wound site, MNs could release antibacterial agents deep inside the biofilm for enhanced therapeutic effect.[38] In this research, hierarchically porous GOx@Fe-ZIF-TA could be used as a glucose-responsive depot to fabricate stimuli-responsive MNs for infected diabetic wound treatment.

As illustrated in Scheme 2, the glucose-responsive MNs were fabricated through a micromolding technique. PVP, as a common biocompatible dissolvable polymer applied in MN systems, was used as the matrix to entrap hierarchically porous GOx@Fe-ZIF-TA. PVA was employed to improve the mechanical properties of MNs.[45] A scanning electron microscope (SEM) and a digital camera were used to image the morphology of MNs. As can be seen from Fig. 3a and b, all MNs displayed a pyramidal structure, and there were 15 × 15 needles on each patch. The total area of MNs was 11 × 11 cm^2. The lateral view of the MNs (Fig. 3c) showed that each needle had a base of 320 μm, and a height of 730 μm. As previous reports demonstrated, 730 μm could be considered to be enough for insertion.[45] As Fig. 3d showed, the distribution of hierarchically porous particles in the needles was confirmed by the green fluorescence of FITC-labeled GOx embedded in GOx@Fe-ZIF-TA, revealing the successful fabrication of glucose-responsive MNs.

To achieve effective penetration, MNs should possess sufficient mechanical strength. In response to this, the MNs were applied onto porcine skin. The microchannel left on porcine skin is shown in Fig. 3e, which indicated that the MNs could effectively penetrate into the wound sites. Also, the mechanical strength of the MNs was measured to be 0.0226 N per needle

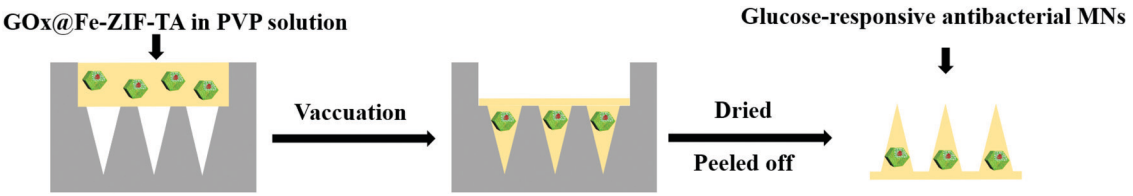

Scheme 2 Schematic illustration of the preparation of MOF-based MNs through micromolding technology.

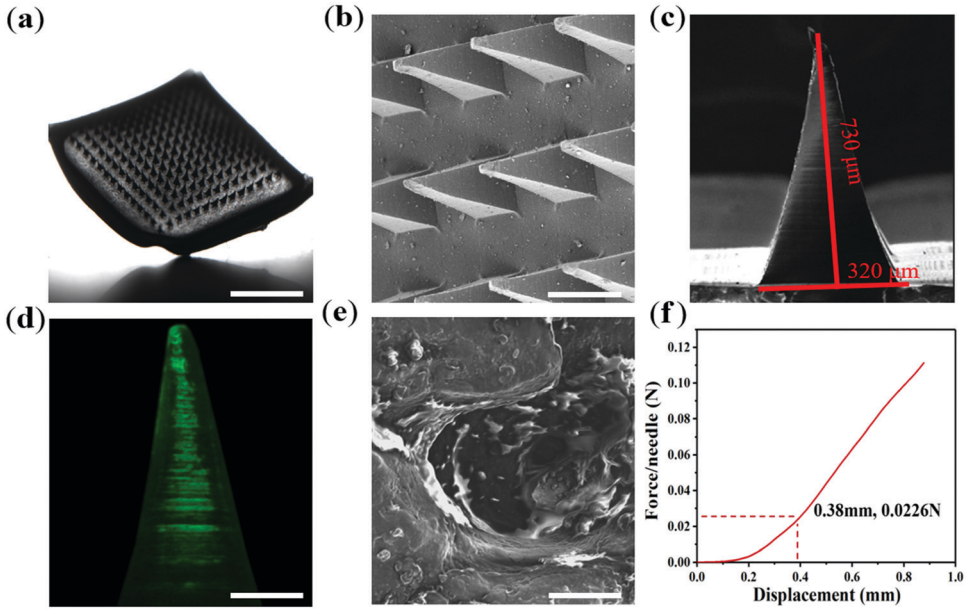

Fig. 3 (a) Digital camera image of MNs with a light source behind the MNs (scale bar: 500 mm). (b) SEM image of MNs (scale bar: 500 μm). (c) Lateral view of MN imaged by SEM. (d) Fluorescence microscopy image of MNs loaded with GOx@Fe-ZIF-TA (GOx modified with FITC, scale bar: 150 μm). (e) SEM image of the microchannel formed on porcine skin (scale bar: 100 μm). (f) Mechanical strength of MNs.

(Fig. 3f), and a force like this was considered to be sufficient for skin penetration.[46]

Conclusions

In summary, hierarchically porous MOF-based stimuli-responsive MNs were designed for infected diabetic wound treatment. A hierarchically porous MOF achieved by a controlled etching process revealed glucose-responsive antibacterial activity, and the as-obtained MNs showed sufficient mechanical strength for the application of transdermal treatment. Our study utilized hierarchically porous MOF-based MNs to offer a promising stimuli-responsive system for infected diabetic wound healing. Furthermore, the facile synthesis of the hierarchically porous MOF for enhanced enzyme-involved catalytic efficiency makes our MOF-based MNs a promising platform that could be expanded into other stimuli-responsive treatments for various diseases.

Conflicts of interest

The authors declare no conflict of interest.

Acknowledgements

We acknowledge the financial support from the National Natural Science Foundation of China (Projects 21871121), the Science and Technological Plan of Gansu Province (20YF3GA012) and the 111 Project (B20027).

References

1 H. Furukawa, K. E. Cordova, M. O'Keeffe and O. M. Yaghi, The chemistry and applications of metal-organic frameworks, *Science*, 2013, **341**, 1230444.
2 J. Dong, D. Zhao, Y. Lu and W.-Y. Sun, Photoluminescent metal–organic frameworks and their application for sensing biomolecules, *J. Mater. Chem. A*, 2019, **7**, 22744–22767.
3 Y. Wang, J. Yan, N. Wen, H. Xiong, S. Cai, Q. He, Y. Hu, D. Peng, Z. Liu and Y. Liu, Metal-organic frameworks for stimuli-responsive drug delivery, *Biomaterials*, 2020, **230**, 119619.
4 X. Cai, Z. Xie, D. Li, M. Kassymova, S. Zang and H. Jiang, Nano-sized metal-organic frameworks: Synthesis and applications, *Coord. Chem. Rev.*, 2020, **417**, 213366.
5 C. Pettinari, R. Pettinari, C. Nicola, A. Tombesi, S. Scuri and F. Marchetti, Antimicrobial MOFs, *Coord. Chem. Rev.*, 2021, **446**, 214121.
6 C. Doonan, R. Ricco, K. Liang, D. Bradshaw and P. Falcaro, Metal-organic frameworks at the biointerface: synthetic strategies and applications, *Acc. Chem. Res.*, 2017, **50**, 1423–1432.
7 X. Lian, Y. Fang, E. Joseph, Q. Wang, J. Li, S. Banerjee, C. Lollar, X. Wang and H. C. Zhou, Enzyme-MOF (metal-organic framework) composites, *Chem. Soc. Rev.*, 2017, **46**, 3386–3401.
8 M. A. Luzuriaga, R. P. Welch, M. Dharmarwardana, C. E. Benjamin, S. Li, A. Shahrivarkevishahi, S. Popal, L. H. Tuong, C. T. Creswell and J. J. Gassensmith, Enhanced stability and controlled delivery of MOF-encapsulated vaccines and their immunogenic response in vivo, *ACS Appl. Mater. Interfaces*, 2019, **11**, 9740–9746.

9 H. An, J. Song, T. Wang, N. Xiao, Z. Zhang, P. Cheng, S. Ma, H. Huang and Y. Chen, Metal-organic framework disintegrants: enzyme preparation platforms with boosted activity, *Angew. Chem., Int. Ed.*, 2020, **59**, 16764–16769.
10 X. Wu, C. Yang, J. Ge and Z. Liu, Polydopamine tethered enzyme/metal-organic framework composites with high stability and reusability, *Nanoscale*, 2015, **7**, 18883–18886.
11 J. Guo, L. Yang, Z. Gao, C. Zhao, Y. Mei and Y. Song, Insight of MOF environment-dependent enzyme activity via MOFs-in-nanochannels configuration, *ACS Catal.*, 2020, **10**, 5949–5958.
12 Y. Guo, Y. Li, S. Zhou, Q. Ye, X. Zan and Y. He, Metal-organic framework-based composites for protein delivery and therapeutics, *ACS Biomater. Sci. Eng.*, 2021, DOI: 10.1021/acsbiomaterials.0c01600.
13 S. Liu, M. Yang and W. Guo, Programmable and reversible regulation of catalytic hemin@MOFs activities with DNA structures, *Chem. Res. Chin. Univ.*, 2020, **36**, 301–306.
14 Z. Zhang, C. Liu, A. Ozioma, W. Xu, A. Wu and Y. Zhang, ICG and sunitinib-loaded NH_2-MOFs for folate-mediated hepatocellular carcinoma dual-modal therapy, *Chem. Res. Chin. Univ.*, 2021, **37**, 967–974.
15 W. H. Chen, G. F. Luo, M. Vazquez-Gonzalez, R. Cazelles, Y. S. Sohn, R. Nechushtai, Y. Mandel and I. Willner, Glucose-responsive metal-organic-framework nanoparticles act as ''smart'' sense-and-treat carriers, *ACS Nano*, 2018, **12**, 7538–7545.
16 L. Zhang, S. S. Wan, C. X. Li, L. Xu, H. Cheng and X. Z. Zhang, An adenosine triphosphate-responsive autocatalytic Fenton nanoparticle for tumor ablation with self-supplied H2O2 and acceleration of Fe(III)/Fe(II) conversion, *Nano Lett.*, 2018, **18**, 7609–7618.
17 X. X. Yang, P. Feng, J. Cao, W. Liu and Y. Tang, Composition-engineered metal-organic framework-based microneedles for glucose-mediated transdermal insulin delivery, *ACS Appl. Mater. Interfaces*, 2020, **12**, 13613–13621.
18 Y. Chen, V. Lykourinou, C. Vetromile, T. Hoang, L. J. Ming, R. W. Larsen and S. Ma, How can proteins enter the interior of a MOF? Investigation of cytochrome *c* translocation into a MOF consisting of mesoporous cages with microporous windows, *J. Am. Chem. Soc.*, 2012, **134**, 13188–13191.
19 Z. Ge, Q. Li and C. Fan, Framework nucleic acids for cell imaging and therapy, *Chem. Res. Chin. Univ.*, 2020, **36**, 1–9.
20 F. K. Shieh, S. C. Wang, C. I. Yen, C. C. Wu, S. Dutta, L. Y. Chou, J. V. Morabito, P. Hu, M. H. Hsu, K. C. Wu and C. K. Tsung, Imparting functionality to biocatalysts via embedding enzymes into nanoporous materials by a de novo approach: size-selective sheltering of catalase in metal-organic framework microcrystals, *J. Am. Chem. Soc.*, 2015, **137**, 4276–4279.
21 K. Liang, R. Ricco, C. M. Doherty, M. J. Styles, S. Bell, N. Kirby, S. Mudie, D. Haylock, A. J. Hill, C. J. Doonan and P. Falcaro, Biomimetic mineralization of metal-organic frameworks as protective coatings for biomacromolecules, *Nat. Commun.*, 2015, **6**, 7240.
22 S. Y. Chen, W. S. Lo, Y. D. Huang, X. Si, F. S. Liao, S. W. Lin, B. P. Williams, T. Q. Sun, H. W. Lin, Y. An, T. Sun, Y. Ma, H. C. Yang, L. Y. Chou, F. K. Shieh and C. K. Tsung, Probing interactions between metal-organic frameworks and free-standing enzymes in a hollow structure, *Nano Lett.*, 2020, **20**, 6630–6635.
23 J. Liang, S. Gao, J. Liu, M. Y. B. Zulkifli, J. Xu, J. Scott, V. Chen, J. Shi, A. Rawal and K. Liang, Hierarchically porous biocatalytic MOF microreactor as a versatile platform towards enhanced multienzyme and cofactor-dependent biocatalysis, *Angew. Chem., Int. Ed.*, 2021, **60**, 5421–5428.
24 C. Avci, J. Arinez-Soriano, A. Carne-Sanchez, V. Guillerm, C. Carbonell, I. Imaz and D. Maspoch, Post-synthetic anisotropic wet-chemical etching of colloidal sodalite ZIF crystals, *Angew. Chem., Int. Ed.*, 2015, **54**, 14417–14421.
25 Y. Sun, J. Shi, S. Zhang, Y. Wu, S. Mei, W. Qian and Z. Jiang, Hierarchically porous and water-tolerant metal–organic frameworks for enzyme encapsulation, *Ind. Eng. Chem. Res.*, 2019, **58**, 12835–12844.
26 H. Wang, W. Zhu, Y. Ping, C. Wang, N. Gao, X. Yin, C. Gu, D. Ding, C. J. Brinker and G. Li, Controlled fabrication of functional capsules based on the synergistic interaction between polyphenols and MOFs under weak basic condition, *ACS Appl. Mater. Interfaces*, 2017, **9**, 14258–14264.
27 M. Hu, Y. Ju, K. Liang, T. Suma, J. Cui and F. Caruso, Void engineering in metal–organic frameworks via synergistic etching and surface functionalization, *Adv. Funct. Mater.*, 2016, **26**, 5827–5834.
28 T. Chung, S. Sevens Jr, F. Lir and C. Wei, Growth inhibition of selected food-borne bacteria by tannic acid, propyl gallate and related compounds, *Lett. Appl. Microbiol.*, 1993, **17**, 29–32.
29 T. Liu, W. Liu, M. Zhang, W. Yu, F. Gao, C. Li, S. B. Wang, J. Feng and X. Z. Zhang, Ferrous-supply-regeneration nanoengineering for cancer-cell-specific ferroptosis in combination with imaging-guided photodynamic therapy, *ACS Nano*, 2018, **12**, 12181–12192.
30 Q. Ouyang, F. Kou, P. E. Tsang, J. Lian, J. Xian, J. Fang and Z. Fang, Green synthesis of Fe-based material using tea polyphenols and its application as a heterogeneous Fenton-like catalyst for the degradation of lincomycin, *J. Cleaner Prod.*, 2019, **232**, 1492–1498.
31 L. Gao, K. M. Giglio, J. L. Nelson, H. Sondermann and A. J. Travis, Ferromagnetic nanoparticles with peroxidase-like activity enhance the cleavage of biological macromolecules for biofilm elimination, *Nanoscale*, 2014, **6**, 2588–2593.
32 B. Xu, H. Wang, W. Wang, L. Gao, S. Li, X. Pan, H. Wang, H. Yang, X. Meng, Q. Wu, L. Zheng, S. Chen, X. Shi, K. Fan, X. Yan and H. Liu, A single-atom nanozyme for wound disinfection applications, *Angew. Chem., Int. Ed.*, 2019, **58**, 4911–4916.
33 W. Clayton and T. A. Elasy, A review of the pathophysiology, classification, and treatment of foot ulcers in diabetic patients, *Clin. Diabetol.*, 2009, **10**, 209–216.

34 P. Bhadauriya, H. Mamtani, M. Ashfaq, A. Raghav, A. K. Teotia, A. Kumar and N. Verma, Synthesis of yeast-immobilized and copper nanoparticle-dispersed carbon nanofiber-based diabetic wound dressing material: simultaneous control of glucose and bacterial infections, *ACS Appl. Bio Mater.*, 2018, **1**, 246–258.
35 M. Wang, L. Hu and C. Xu, Recent advances in the design of polymeric microneedles for transdermal drug delivery and biosensing, *Lab Chip*, 2017, **17**, 1373–1387.
36 S. Yao, J. Chi, Y. Wang, Y. Zhao, Y. Luo and Y. Wang, Zn-MOF encapsulated antibacterial and degradable microneedles array for promoting wound healing, *Adv. Healthcare Mater.*, 2021, **10**, e2100056.
37 S. Esposito, T. Ascione and P. Pagliano, Management of bacterial skin and skin structure infections with polymicrobial etiology, *Expert Rev. Anti-Infect. Ther.*, 2019, **17**, 17–25.
38 R. Jamaledin, C. K. Y. Yiu, E. N. Zare, L. N. Niu, R. Vecchione, G. Chen, Z. Gu, F. R. Tay and P. Makvandi, Advances in antimicrobial microneedle patches for combating infections, *Adv. Mater.*, 2020, **32**, 2002129.
39 M. Chen, G. Quan, Y. Sun, D. Yang, X. Pan and C. Wu, Nanoparticles-encapsulated polymeric microneedles for transdermal drug delivery, *J. Controlled Release*, 2020, **325**, 163–175.
40 H. Zhang, S. Hwang, M. Wang, Z. Feng, S. Karakalos, L. Luo, Z. Qiao, X. Xie, C. Wang, D. Su, Y. Shao and G. Wu, Single atomic iron catalysts for oxygen reduction in acidic media: particle size control and thermal activation, *J. Am. Chem. Soc.*, 2017, **139**, 14143–14149.
41 V. Lykourinou, Y. Chen, X. S. Wang, L. Meng, T. Hoang, L. J. Ming, R. L. Musselman and S. Ma, Immobilization of MP-11 into a mesoporous metal-organic framework, MP-11@mesoMOF: a new platform for enzymatic catalysis, *J. Am. Chem. Soc.*, 2011, **133**, 10382–10385.
42 Q. Wang, S. Tian and P. Ning, Degradation mechanism of methylene blue in a heterogeneous Fenton-like reaction catalyzed by ferrocene, *Ind. Eng. Chem. Res.*, 2013, **53**, 643–649.
43 A. Üçer, A. Uyanik and Ş. F. Aygün, Adsorption of Cu(II), Cd(II), Zn(II), Mn(II) and Fe(III) ions by tannic acid immobilised activated carbon, *Sep. Purif. Technol.*, 2006, **47**, 113–118.
44 Y. Wu, R. Yan, Y. Duan, J. Qiu, T. Chen and H. Ma, An environmental-friendly tannic acid/Zn conversion film with a good corrosion protection for iron, *Surf. Interfaces*, 2021, **24**, 101078–101086.
45 I. C. Lee, J. S. He, M. T. Tsai and K. C. Lin, Fabrication of a novel partially dissolving polymer microneedle patch for transdermal drug delivery, *J. Mater. Chem. B*, 2015, **3**, 276–285.
46 S. D. Gittard, B. Chen, H. Xu, A. Ovsianikov, B. N. Chichkov, N. A. Monteiro-Riviere and R. J. Narayan, The effects of geometry on skin penetration and failure of polymer microneedles, *J. Adhes. Sci. Technol.*, 2013, **27**, 227–243.

